DEVELOPMENT OF SURFACE WAVE DISPERSION AND ATTENUATION MAPS AND IMPROVED METHODS FOR MEASURING SURFACE WAVES

Jeffry L. Stevens, Jeffrey W. Given, G. Eli Baker and Heming Xu

Science Applications International Corporation

Sponsored by Air Force Research Laboratory

Contract No. FA8718-05-C-0023

ABSTRACT

The objective of this project is to optimize measurement of surface waves, particularly at regional and local distances and at periods of 8–15 s. An important part of the project is the development of global regionalized dispersion and attenuation maps, with a particular focus on determining attenuation maps for Eurasia in the 8–15 s period band. Both the dispersion and attenuation maps are corrected for scattering and diffraction from heterogeneous earth structure, and amplitude correction "maps" are also being developed.

Surface wave propagation in the frequency band of interest is strongly affected by heterogeneous earth structure as well as attenuation, particularly along paths crossing deep sedimentary basins. Two such basins of interest in Eurasia are the Tarim Basin in Western China, and the West Siberian Basin. Explosions within these basins generate unusually high amplitude and persistent high frequency fundamental mode surface waves. The Quartz3 and Kimberlite peaceful nuclear explosions (PNEs) were conducted in the West Siberian Basin, and their data give a particularly good sampling of the surface wave propagation across the basin, so we are analyzing these events in detail.

We implemented the algorithm of Zhou et al. (2004) for calculating finite frequency sensitivity kernels for dispersion and amplitude variations, and have been testing the algorithms using the one-degree dispersion maps of Stevens et al. (2005). We performed a large test inversion similar to our earlier great circle path inversions, but using the finite frequency sensitivity kernels. While the inversion looks reasonable, it is not yet clear whether the results fit the data significantly better than the simpler great-circle representation. Amplitude corrections predicted by the Born approximation for the one degree model seem unreasonably large on long paths. This likely reflects the limit of the approximation when large velocity contrasts are encountered.

In order to validate and improve the results, we test whether the Born approximation is giving correct results for structural variations of the magnitude present in the Stevens et al. (2005) models at the frequencies of interest. We compare theoretical Rayleigh wave spectra derived using the Born approximation with those calculated by a 3D finite difference method. The test model was the Tarim Basin structure embedded in a uniform structure typical of the Eurasian shield regions. The source was located immediately east of the basin and the predicted wavefields were compared out to several hundred km west of the basin. The Born approximation is generally consistent with the finite-difference results, but there are localized, strong interference effects in the finite-difference results not apparent in the Born calculation. As expected, the approximation is less accurate at 10 s periods than at 20 s because of the larger phase velocity variation at shorter periods.

We define a path corrected time domain magnitude, which combines the time domain narrow-band surface wave magnitude procedure of Russell (2006) with the path corrected spectral magnitude of Stevens and McLaughlin (2001). The dispersion and attenuation corrections being developed in this project will be used to define regionalized correction factors for this magnitude.

OBJECTIVES

The objective of this project is to optimize measurement of surface waves, particularly at regional and local distances and at periods of 8–15 s. An important part of the project is the development of global regionalized dispersion and attenuation maps, with a particular focus on determining attenuation maps for Eurasia in the 8–15 s period band. Both the dispersion and attenuation maps are being corrected for scattering and diffraction from heterogeneous earth structure.

RESEARCH ACCOMPLISHED

Overview

Surface wave amplitudes are affected by both attenuation and earth structure. The effect on surface wave amplitudes of propagation normal to variations in earth structure is predicted fairly well by energy conservation. Propagation along paths at grazing incidence to large structure variations, however, are much more difficult to predict. Our main interest in this project is on understanding amplitude variations in 8–15 s surface waves. In this frequency band, surface waves may be affected as strongly or more strongly by earth structure than by intrinsic attenuation, particularly along shorter paths. Our goal is therefore to be able to model and correct for both of these effects. Our plan for doing so is illustrated in Figure 1.

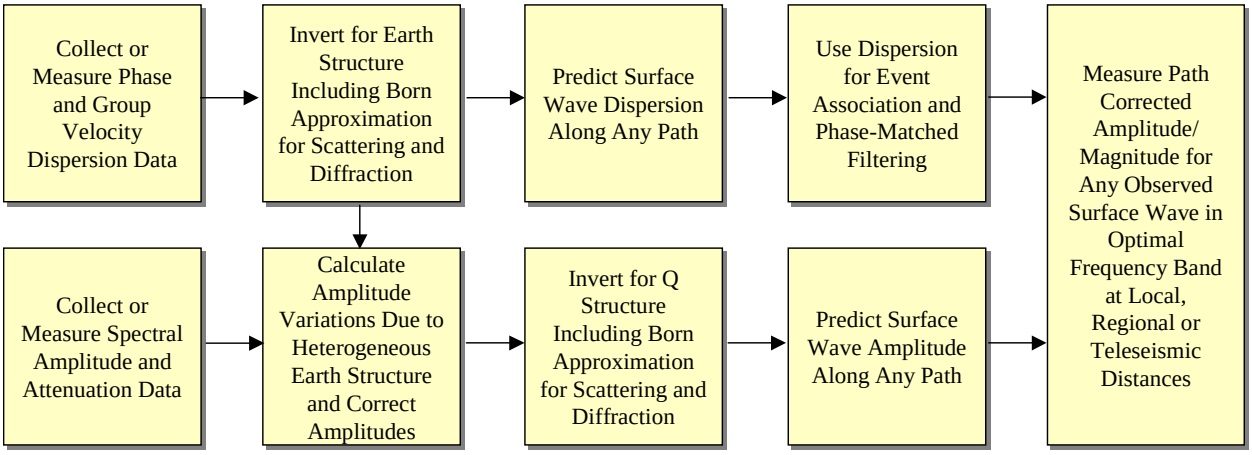

Figure 1. Overview of the surface wave dispersion and attenuation project.

In an earlier project (Stevens et al., 2005) we developed global, regionalized dispersion models that allow the phase and group velocity to be calculated between any two points on the earth. We did this by accumulating a large data set consisting of more than one million dispersion measurements derived by a number of researchers, and then inverting this data set to determine earth structure, which in turn was used to generate dispersion maps at all frequencies. In that project, we modeled surface waves in a heterogeneous earth using the following approximations: (1) surface waves propagate along great circle paths, (2) surface wave phase and group velocities and anelastic attenuation can be modeled using a path integral between source and receiver, and (3) energy is conserved with no mode conversion across material boundaries. This approximation is quite good for large parts of the world, particularly at lower frequencies, but the unmodeled variations become important in regions of structural complexity.

In the first year of this project, we have focused on understanding the variations in surface wave dispersion and amplitude caused by heterogeneous earth structure. We have recalculated our tomographic inversions using finite frequency Born sensitivity kernels in place of the great circle path integrals. We have calculated amplitude variations along Eurasian paths using the resulting earth models, again using the Born approximation to calculate amplitude variations. We are looking in detail at surface waves propagating in highly heterogeneous regions, and trying to understand and model their behavior. Two particularly heterogeneous areas in Eurasia are the Siberian Basin and the Tarim Basin, and so we have been analyzing surface waves in these areas in detail. Our plan is to

develop Born amplitude corrections first, to assess their performance by comparison with data, and then to incorporate the amplitude corrections into inversions for surface wave attenuation. The combination of the attenuation correction and amplitude corrections is necessary to allow accurate prediction of surface wave amplitudes.

Surface Wave Amplitude Predictability

An important goal of this project is to be able to predict surface wave amplitudes in both simple and complex structures, to determine under what conditions the more complicated calculations for laterally heterogeneous structure are required, and under what conditions the approximations generally used for calculating surface waves in complex structures become inadequate. In the following, we discuss calculations of surface waves in simple and complex structures.

Surface Wave Propagation in Simple Structures

We define "simple structures" to mean those structures in which the surface wave propagation is normal to all changes in structure, and lateral changes in structure are negligible. In that case we can predict surface wave amplitude and phase using an approximation originally due to McGarr (1969) that uses propagation of surface waves along great circle paths with conservation of energy across material interfaces and no mode conversion. With these approximations, surface wave propagation in a heterogeneous, anelastic structure takes the following form, separating source, path and receiver (notation follows Harkrider et al, 1994):

$$u_z(\omega,r,\varphi) = \frac{1}{\sqrt{a_e \sin\left(r/a_e\right)}} \sqrt{\frac{2A_{R_1}}{\pi\omega c_1^{\,2}}} \sqrt{c_2 A_{R_2}} \exp\left[i\left(\pi/4 - \omega r / c_p - \gamma_p r\right)\right] F_s(\omega,\varphi,h) \ , \qquad \textbf{(1)}$$

where ω is angular frequency, r is source to receiver distance, h is source depth, a_e is the radius of the earth, φ is azimuth, A_R is the Rayleigh wave amplitude function, c is phase velocity, γ is the attenuation coefficient, and the subscripts *1*, *2*, and *p* refer to parameters derived from the source region structure, parameters derived from the receiver region structure, and parameters which are defined by path averages, respectively. All source properties are contained in the function F_s. For an isotropic explosion source, the Rayleigh wave spectrum can be written:

$$u_z(\omega,r) = M_0^{'} \frac{S_1^x(\omega,h_x) S_2(\omega) \exp[-\gamma_p(\omega) r + i(\varphi_0 - \omega r / c_p(\omega))]}{\sqrt{a_e \sin(r/a_e)}} \ , \qquad (2)$$

where φ_0 is the initial phase equal to -3π/4, S_1^x depends on the source region elastic structure and the explosion source depth, and S_2 depends on the receiver region elastic structure. $M_0^{'} = \frac{3\beta^2}{\alpha^2} M_0$ where M_0 is the explosion isotropic moment. $M_0^{'}$ is defined this way so that the function S_1^x does not depend explicitly on the material properties at the source depth. More details are given in Stevens and McLaughlin (2001) and Stevens and Murphy (2001).

Surface Wave Propagation in Complex Structures

In more complex structures, Equations (1) and (2) may be inadequate to describe surface waves. Consequently, we have been testing algorithms that may be more appropriate for these structures. We implemented the algorithms of Zhou et al. (2004) for calculating finite frequency sensitivity kernels for dispersion and amplitude variations. Using the forward scattering, forward propagating approximation, the phase and amplitude corrections are:

$$\delta\phi = \iint K_\phi^c \left(\delta c/c\right) d\Omega \ , \text{ where } \ K_\phi^c = -\frac{2k^{3/2} \sin\left[k\left(\Delta' + \Delta'' - \Delta\right) + \pi/4\right]}{\sqrt{8\pi \sin\Delta' \sin\Delta''/\sin\Delta}} \ \text{ and} \qquad (3)$$

$$\delta \ln A = \iint K_A^c \left(\delta c/c\right) d\Omega \ , \text{ where } K_A^c = -\frac{2k^{3/2} \cos\left[k\left(\Delta' + \Delta'' - \Delta\right) + \pi/4\right]}{\sqrt{8\pi \sin\Delta' \sin\Delta''/\sin\Delta}} \ , \qquad (4)$$

where distance is in radians, k is wavenumber, and Δ', Δ" and Δ refer to the source to scatterer, scatterer to receiver, and source to receiver distances, respectively. The integrals run over the entire earth's surface, although in practice

(and in this paper) are limited to the first Fresnel zone, which is defined by $k(\Delta' + \Delta'' - \Delta) < 3\pi/4$. Dahlen and Zhou (2006) extend these equations to derive group delay and intrinsic attenuation kernels.

Application of Corrections to Surface Wave Amplitudes

We have been testing the algorithms described above using the 1 degree dispersion maps of Stevens et al. (2005). While the results are reasonable for prediction of dispersion variations, the predicted amplitude corrections seem unreasonably large, particularly on long paths. Consequently, we have been investigating how model roughness affects amplitudes. Figure 2 shows the 10 s phase velocity model for Eurasia; Figure 3 shows the predicted amplitude variation for paths through this region from the Lop Nor test site using the model shown in Figure 2 directly, and using a "smoothed" version of the amplitude variation in which the phase slowness was modeled with a bilinear function instead of discrete blocks. For both of the amplitude figures, the anomalies have been truncated where they exceed $\log_{10}$(amplitude) = 0.6. The amplitude variations become quite large on longer paths, and it is not clear whether the Born approximation is giving reasonable answers on these paths.

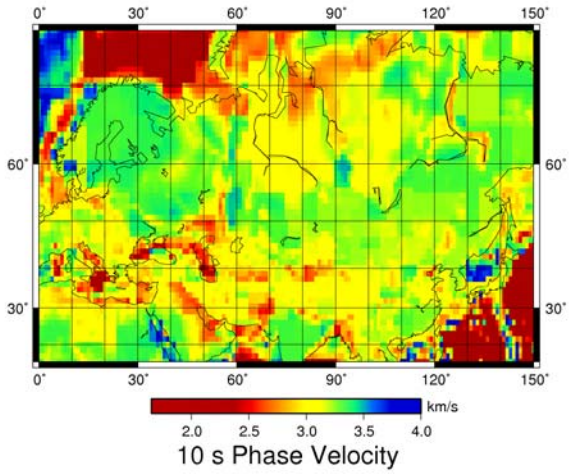

Figure 2. Eurasian phase velocity model at 10 s from Stevens et al. (2005).

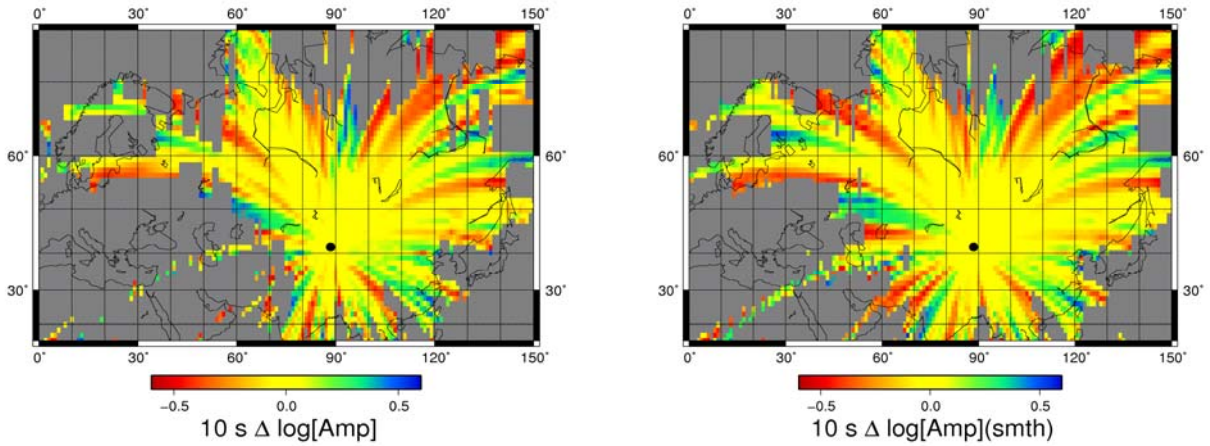

Figure 3. Left—predicted amplitude variations at 10 s through the phase velocity model of Figure 2 on paths out of Lop Nor. Right—same, but the velocity model has been smoothed by modeling it as a bilinear rather than piecewise discontinuous function.

In order to validate/correct the results, we need to determine whether the Born approximation is giving correct results for structural variations of the magnitude present in the Stevens et al. (2005) models, and at the frequencies of interest. To do this, we performed a test case of a structure for the Tarim Basin embedded in a uniform structure typical of shield regions of Eurasia, such as those that surround the Tarim Basin (Figure 4). We then performed a Born approximation calculation and a 3D finite difference calculation for a source located just east of the Tarim Basin and examined the wavefield for several hundred km west of the Tarim Basin. The results showed that although the Born approximation is generally consistent with the finite difference results, there are noticeable interference effects leading to high and low amplitudes in the finite difference calculation that are not present in the Born approximation. The differences are significantly larger at 10 s than at 20 s.

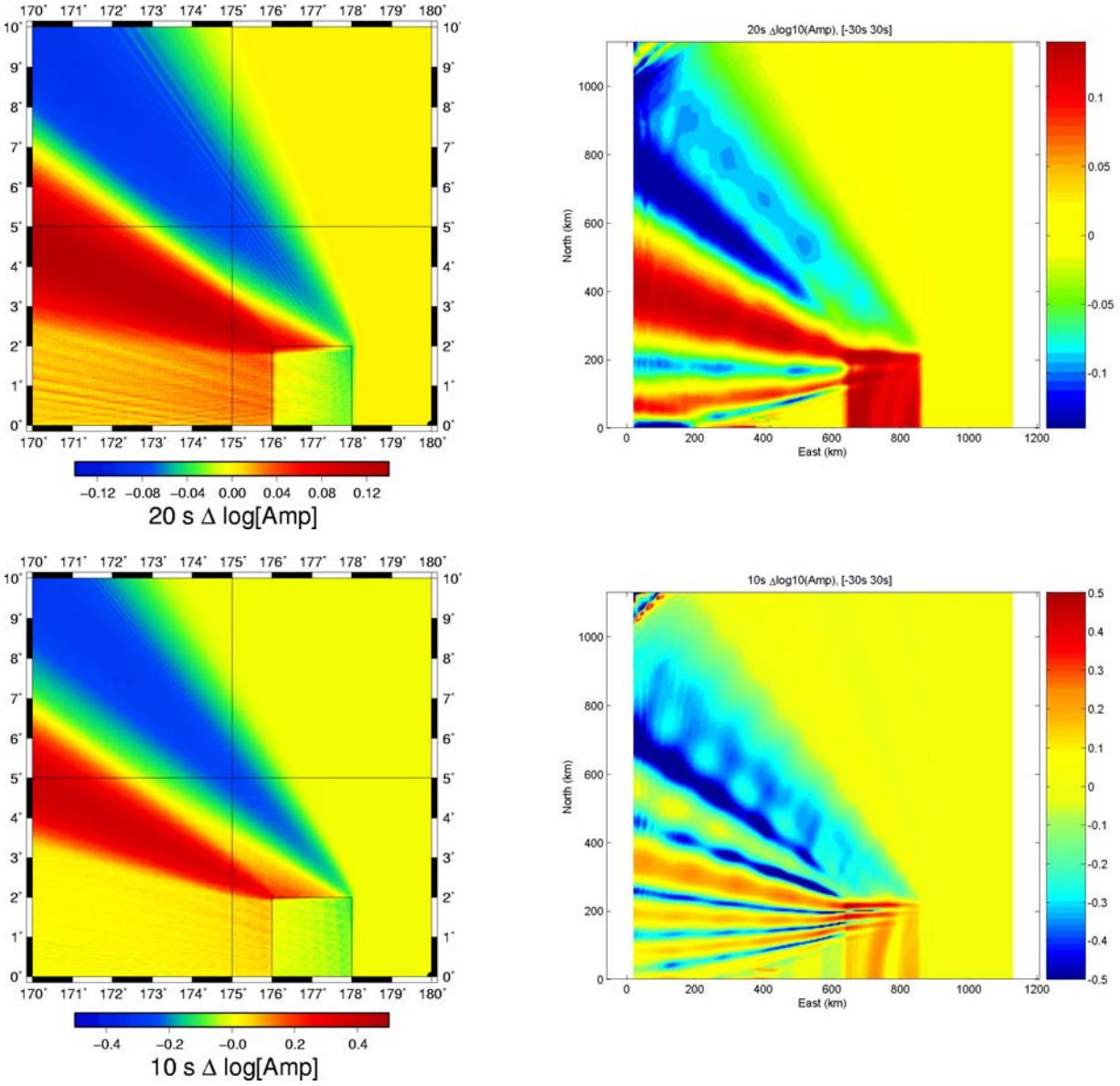

Figure 4. Comparison of Born approximation (left) with finite difference calculation (right) of amplitude perturbations at 20 s (top) and 10 s (bottom). The rectangular inclusion is modeled after the Tarim Basin structure, and the external structure after a Eurasian shield earth structure. The source is on the horizontal axis at the right edge of the plot. There is general agreement in the features of the two calculations. The amplitude is increased in a band above and to the left of the inclusion in both cases, and decreased above that. However, there are some interference effects in the finite difference calculation that are not reproduced in the Born calculation.

One reason for this increase in complexity is illustrated in Figure 5. Propagation of the cylindrical wave leaving the source through the Tarim Basin model leads to a strong diffracted wave generated by the wavefront passing along the top of the basin. This secondary wave interferes with the direct wave and complicates analysis, particularly in the interpretation of spectra. Since the first order Born approximation only models the direct wave, it cannot reproduce this strongly diffracted secondary wave, although it may do an adequate job of predicting the primary arrival. Also shown in Figure 5 are two observed waveforms that traveled through the Tarim Basin. There are two distinct surface wave arrivals similar to the figure on the left. Although we have not done sufficient analysis to say that the split in these seismograms was due to the effect illustrated in the left figure, it does suggest that strong diffraction may be responsible.

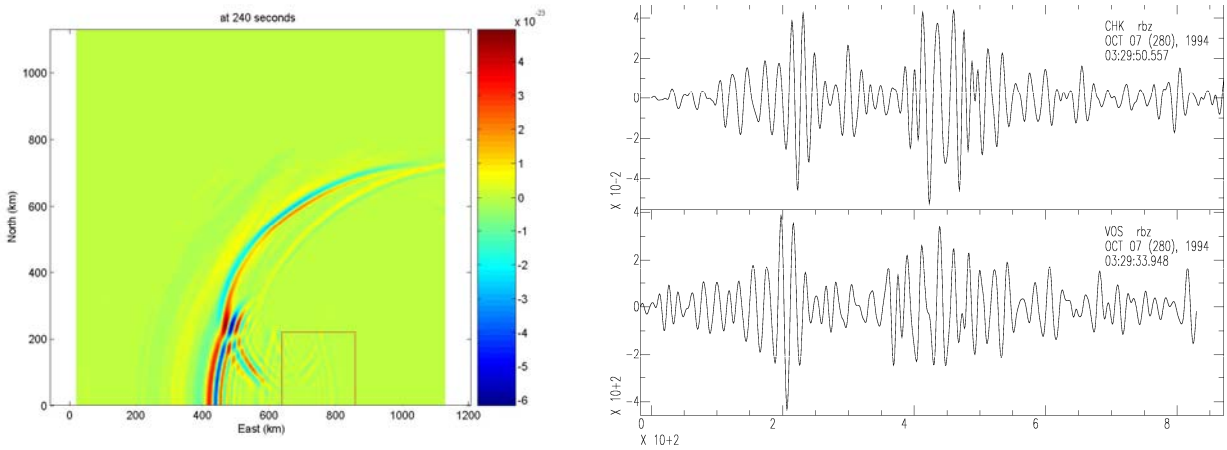

Figure 5. Vertical component velocity after propagation across the low velocity basin (left). There is a strong diffracted wave that interferes with the direct wave. The right figure shows two observed waveforms that passed through the Tarim Basin and have two distinct surface wave arrivals.

Application of Corrections to Inversion for Earth Structure

As discussed earlier, our plan is to incorporate Born corrections for scattering and diffraction into our tomographic inversion scheme. Although we are primarily interested in amplitude estimates, it is necessary to first recalculate the dispersion inversions for earth structure in order to account correctly for the structural effects on amplitude. We have incorporated the finite frequency sensitivity kernels (Equation 3) into our inversion code, and rerun the global tomographic inversions (Stevens et al., 2005) with these corrections. As of this writing, we are still evaluating the results. The changes from the previous inversion are modest in most areas, so more analysis is needed to determine whether results represent an improvement over the inversion using great circle paths. We anticipate that the inversions will give more realistic earth structure with slightly improved data fits in areas of strong lateral heterogeneity.

Data Analysis

We have been identifying data sets in Eurasia that can be used to determine attenuation, as well as dispersion, from 5 to 20 s surface waves. These data sets include nuclear test data, PNEs of the former Soviet Union, moderate size earthquakes recorded at the International Monitoring System (IMS) stations with Harvard Centroid Movement Tensor (CMT) solutions, and deep seismic sounding (DSS) data. The DSS data are potentially very interesting, even though the instrument response of the short period geophones used in those studies is not optimal for longer period (~10–20 s) surface waves. Two of the DSS explosions, Kimberlite 1 (8.5 kt) and Quartz 3 (22 kt), were detonated within the Siberian Basin, and showed very strong surface waves along the entire seismic line, even at long periods. Recordings of both events outside of the basin at 3,300 km, at the very quiet IRIS/GSN station KONO, have surface waves of the amplitude expected from 8.5 and 22 Kt explosions at that distance. This suggests that long period site amplifications may be especially high within the basin. Figure 6 shows data from Kimberlite 1 recorded at 349 km, in 5 passbands (left) and synthetics for a basin structure (right). An interesting characteristic of the data that can be

seen in this figure is that while the synthetic seismogram exhibits smoothly increasing dispersion between low and high frequencies, the data show more of a discontinuous jump. That is, the Rg data near 1 Hz is consistent with the synthetic, and the main arrival of the long period surface wave at the lowest frequencies is also consistent with the synthetic, however there is not a smooth transition between them. Instead, the Rg and long period surface waves or appears almost as two distinct phases, with the long period part of the data growing with decreasing frequency and the Rg decreasing with decreasing frequency.

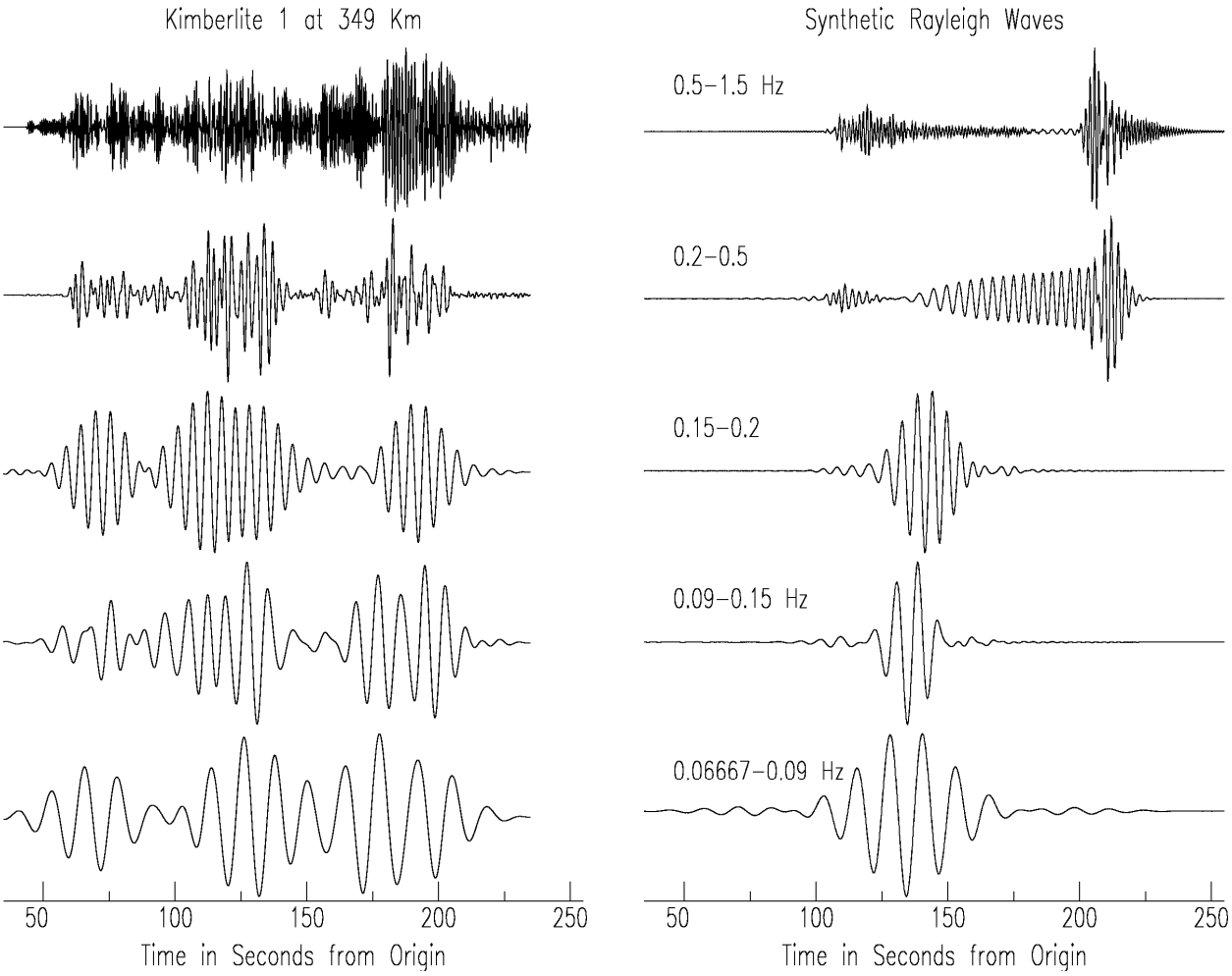

Figure 6. Vertical component Kimberlite-1 record at 349 km (left) in 5 passbands (centered approximately on 1, 3.5, 6, 9, and 13 s from top down), and corresponding synthetics for the first five modes for a Siberian Basin structure.

Regionalization and Improvement of Surface Wave Magnitudes

Regionalization of earth structure, dispersion, and attenuation allows surface wave magnitude estimates to be made more consistent by taking into account regional differences. In addition, consistent surface wave measurement at short distances requires a different procedure than has traditionally been used. Surface wave measurements have typically been made by measuring a time domain amplitude at a period near 20 s and then calculating a surface wave magnitude M_s. This procedure is problematic at regional distances because the surface wave is not well dispersed and a distinct 20 s arrival may not be present. It is possible to measure time domain amplitudes at higher frequencies with corrections (e.g. Marshall and Basham, 1972), however measurements may be inaccurate due to differences in dispersion caused by differences in earth structure. Stevens and McLaughlin (2001) suggested as an alternative replacing time domain measurements with a path corrected spectral magnitude. Russell (2006) proposed a time domain magnitude based on a Butterworth filtered signal, which similarly removes many of the problems associated with time domain magnitudes at close distances. In the following, we suggest a regionalized version of the Russell magnitude which then corresponds to a path corrected time domain magnitude.

Path Corrected Spectral Magnitudes

The path corrected spectral magnitude, $\log M_0$, is calculated by dividing the observed surface wave spectrum by the Green's function for an explosion of unit moment and taking the logarithm of this ratio, averaged over any desired frequency band. The path corrected spectral magnitude is defined as the logarithm of:

$$M_0^{'} = \left| U(\omega, r, \theta) \Big/ \left(\frac{S_1^x(\omega, h_x) S_2(\omega) \exp[-\gamma_p(\omega) r]}{\sqrt{a_e \sin(r / a_e)}} \right) \right|, \tag{5}$$

where U is the observed surface wave spectrum, and as above S_1^x depends on the source region elastic structure and the explosion source depth, S_2 depends on the receiver region elastic structure, and γ_p is the attenuation coefficient that depends on the attenuation integrated over the path between the source and receiver. All of the functions in equation 5 are easily derived from plane-layered earth models (Stevens and McLaughlin, 2001) and allow the measurement to be regionalized to account for differences in earth structure at the source and receiver and due to attenuation along the path. Regionalized path corrected spectral magnitudes incorporate geographic variations in source excitation and attenuation. It can be measured over different frequency bands to optimize the signal-to-noise ratio. M_s and $\log M_0$ share some limitations: spectra from earthquakes vary due to source mechanism and depth, and errors can occur if the measurement is made in a spectral dip or at high frequencies for a deep event. Azimuthal variations in amplitude caused by focal mechanism also affect the amplitudes of both $\log M_0$ and M_s. $\log M_0$ can also be corrected for structural heterogeneity using the amplitude corrections described earlier.

Path Corrected Time Domain Magnitudes

Russell (2006) proposed a new type of surface wave magnitude $M_{s(b)}$ which differs from a traditional 20 s magnitude in that it uses a Butterworth filter to measure a time domain amplitude in a narrow band around any desired frequency, and then applies a correction for the source function similar to the explosion source function used in the path corrected spectral magnitude described above. The main purpose of $M_{s(b)}$ is to allow surface waves to be measured at regional distances at higher frequencies. Bonner et al. (2006) showed that it gave consistent results in a test study. The magnitude is defined by

$$M_{s(b)} = \log(A_b) + \frac{1}{2}\log(\sin\Delta) + 0.0031\left(\frac{20}{T}\right)^{1.8}\Delta - 0.66\log\left(\frac{20}{T}\right) - \log(f_c) - 0.43, \tag{6}$$

where A_b is the filtered amplitude, T is the measured period, and f_c is the Butterworth filter width. It is instructive to compare the terms in the Russell magnitude with the Rezapour and Pearce (1998) M_s and the path corrected spectral magnitude $\log M_0$ described above. This is shown in Table 1.

Table 1. Comparison of time domain and spectral magnitude measurement and correction terms

Magnitude Type	Amplitude Measure	Source	Receiver	Geometric Spreading	Attenuation	Dispersion	Filter	Norm
M_s	log(A/T)			$\frac{1}{2}\log(\sin\Delta)$	0.0046Δ	$\frac{1}{3}\log\Delta$		2.37
$M_{s(b)}$	$\log(A_b)$	$-0.66\log\left(\frac{20}{T}\right)$		$\frac{1}{2}\log(\sin\Delta)$	$.0031\left(\frac{20}{T}\right)^{1.8}\Delta$		$-\log(f_c)$	-0.43
$\log M_0$	$\log(U_z)$	$-\log(S_1)$	$-\log(S_2)$	$\frac{1}{2}\log(\sin\Delta)$	$\gamma_p\Delta\log e$			$\frac{1}{2}\log a_e$

Note that each magnitude makes a slightly different set of corrections. $\log M_0$ corrects for both source and receiver structure based on earth models at those locations and an explosion Green's function at the source. Similarly, $M_{s(b)}$ applies a source correction based on typical explosion source excitation. The Airy phase dispersion correction accounts for superposition of waves with similar group velocities, and is needed only in the time domain. $M_{s(b)}$ uses a Butterworth filter that is sufficiently narrow to avoid this problem. The filter correction corrects for the width of the Butterworth filter. The normalization for the two M_s measurements is chosen to make it consistent with historical M_s magnitudes at a chosen distance range. $\log M_0$ has natural units of log moment and is not otherwise normalized; however, Stevens and McLaughlin (2001) showed that subtracting 11.75 makes $\log M_0$ consistent with the Rezapour and Pearce M_s. Attenuation for M_s is an empirical correction based on a very large number of 20 s measurements. $M_{s(b)}$ similarly uses an empirical attenuation correction, but also includes an empirical correction for the change in attenuation with frequency; $\log M_0$ uses attenuation calculated from earth (velocity, density, and Q) models along a source to receiver path.

A path corrected time domain magnitude can be derived by combining the path corrected spectral magnitude with $M_{s(b)}$, using the source and path corrections from earth models to replace the empirical average corrections. We define the path corrected time domain magnitude $M_{s(bp)}$ as

$$M_{s(bp)} = \log(A_b) + \frac{1}{2}\log(\sin\Delta) + \gamma_p\Delta\log e - \log(S_1) - \log(S_2) - \log(f_c) + C_{bp}, \quad (7)$$

where C_{bp} is a constant chosen to make $M_{s(bp)}$ consistent with historical magnitudes. Although equation 7 may appear more complicated than equation 6, the functions S_1, S_2, and γ_p are easily tabulated and stored in files, and a computer can quickly calculate them for any path based on a simple lookup table. There is substantial regional variation in these quantities that should be removed to ensure consistent measurements (examples of S_1, S_2, and γ for continental and oceanic structures are shown in Stevens and McLaughlin, 1996). Another advantage of this approach is that it can ensure that f_c, which must be less than a minimum value calculated from the group velocity ($f_c < 0.6/\left(T\sqrt{\Delta}\right)$, delta in degrees) is always set appropriately.

None of the magnitude measurements described above include correction for amplitude variations caused by laterally heterogeneous earth structure. To do so requires an additional term that depends on the earth structure in the Fresnel zone surrounding the source to receiver path. The extra term can in principle be calculated using Equation 4, although as discussed previously, the accuracy of this correction particularly for long paths and complex structures requires further investigation.